4274–4283 *Nucleic Acids Research, 2015, Vol. 43, No. 8* *Published online 27 March 2015*
doi: 10.1093/nar/gkv187

Distribution of DNA-condensing protein complexes in the adenovirus core

Ana J. Pérez-Berná[1,2], Sanjin Marion[3], F. Javier Chichón[1,2], José J. Fernández[1], Dennis C. Winkler[4], José L. Carrascosa[1,2], Alasdair C. Steven[4], Antonio Šiber[3,5,*] and Carmen San Martín[1,2,*]

[1]Department of Macromolecular Structures, Centro Nacional de Biotecnología (CNB-CSIC), 28049 Madrid, Spain, [2]NanoBiomedicine Initiative, Centro Nacional de Biotecnología (CNB-CSIC), 28049 Madrid, Spain, [3]Institute of Physics, Bijenička cesta 46, HR-10000 Zagreb, Croatia, [4]Laboratory of Structural Biology, National Institute of Arthritis and Musculoskeletal and Skin Diseases (NIAMS), NIH, Bethesda, MD 20892, USA and [5]Jožef Stefan Institute, Jamova 39, SI-1000 Ljubljana, Slovenia

Received December 12, 2014; Revised February 05, 2015; Accepted February 22, 2015

ABSTRACT

Genome packing in adenovirus has long evaded precise description, since the viral dsDNA molecule condensed by proteins (core) lacks icosahedral order characteristic of the virus protein coating (capsid). We show that useful insights regarding the organization of the core can be inferred from the analysis of spatial distributions of the DNA and condensing protein units (adenosomes). These were obtained from the inspection of cryo-electron tomography reconstructions of individual human adenovirus particles. Our analysis shows that the core lacks symmetry and strict order, yet the adenosome distribution is not entirely random. The features of the distribution can be explained by modeling the condensing proteins and the part of the genome in each adenosome as very soft spheres, interacting repulsively with each other and with the capsid, producing a minimum outward pressure of ∼0.06 atm. Although the condensing proteins are connected by DNA in disrupted virion cores, in our models a backbone of DNA linking the adenosomes is not required to explain the experimental results in the confined state. In conclusion, the interior of an adenovirus infectious particle is a strongly confined and dense phase of soft particles (adenosomes) without a strictly defined DNA backbone.

INTRODUCTION

Regulation of dsDNA condensation is crucial for the management of genetic information throughout Nature. Supercoiling and attractive forces originated by molecular crowding play key roles in this process (1). Molecular crowding contributes to the organization of nuclear compartments and chromosome compaction during metaphase (2,3). A third major player in genome compaction is the action of specialized, positively charged DNA binding proteins. According to their architectural role, these have been classified as benders (bending DNA away from or around themselves), wrappers (folding the DNA around their surface) or bridgers (forming dynamic cross-links between DNA duplexes) (4). Different biological entities use different approaches to condense DNA (5). Supercoiling is predominant in the circular genomes of bacteria, aided by nucleoid-associated proteins with mainly bending and bridging roles. In eukaryotes, wrapping by histones is an essential genome condensation mechanism and the first organizational level of chromatin. Approximately 150 bp of DNA wrap around a histone octamer composed by histones H2A, H2B, H3 and H4 to form the nucleosome core particle, while the bridging protein, linker histone H1, clasps linker DNA at the nucleosome exit, stabilizing the structure. Nucleosomes form a 10-nm beaded fiber that is further compacted into the different states of chromatin throughout the cell cycle. How this higher order of compaction occurs is still under debate (6,7). This fundamental issue is directly related to the interactions between nucleosomes in the crowded nuclear environment.

The degree of DNA condensation is maximal in viruses, where genomes are packaged to near-crystalline densities of up to ∼400 mg/ml (5,8). In some dsDNA viruses (herpesviruses and tailed bacteriophage), the naked genomes become coiled into concentric spool-like structures (9). Polyamines and cations help to relieve the electrostatic repulsion between DNA strands in these highly crowded conditions. Other viruses hijack cellular histones (10) or pro-

*To whom correspondence should be addressed. Tel: +34 91 5855450; Fax: +34 91 5854506; Email: carmen@cnb.csic.es
Correspondence may also be addressed to Antonio Šiber. Tel: +385 1 469 8888; Fax: +385 1 469 8889; Email: asiber@ifs.hr
Present address: Ana J. Pérez-Berná, ALBA Synchrotron Light Source, MISTRAL Beamline Experiments Division, 08290 Cerdanyola del Vallès, Barcelona, Spain.

duce their own histone-like proteins. This last category, probably the least studied case of dsDNA compaction, includes the human pathogen adenovirus.

The interest in adenoviruses is diverse (11). In medicine they are investigated as infective particles causing typically mild diseases, but also as vectors for vaccine and gene delivery and oncolysis (12). Adenoviruses are among the largest non-enveloped icosahedral viruses (vertex to vertex diameter ≈95 nm). They have been found in a wide range of vertebrates, but the most studied are those infecting humans, in particular human adenovirus type 5 (HAdV-C5). The HAdV-C5 icosahedral T = 25 capsid shell is composed of 240 hexon trimers, 12 penton-base pentamers, 12 penton base-associated fiber trimers and four minor coat proteins (IIIa, VI, VIII and IX) (13). Due to the unavoidable influence of icosahedral symmetry in structural studies, information on the non-icosahedrally ordered viral components is scarce. These components play critical roles in the viral cycle, as they include the viral genome and a large entourage of bound proteins (14). A characteristic feature of adenovirus is that positively charged proteins of viral origin (V, VII, μ) cover the 35 kbp dsDNA and are thought to neutralize its negative charge, so that it can be tightly condensed in the viral core within the icosahedral shell.

Polypeptides V, VII and μ have a high proportion of basic residues that makes them similar to histones. They bind dsDNA non-specifically via multiple sites and can condense it in solution (15–19). Polypeptide VII (22 kDa, 21% Arg and 3% Lys) is the major core protein, with estimates ranging between 500 and 800 copies per virion (20,21). Both the precursor and mature forms of polypeptide VII induce supercoiling in relaxed closed circular dsDNA in the presence of cellular chromatin extract (22). There are ∼150 copies of the minor core protein V (41 kDa, 13% Arg and 7% Lys) per virion. Apart from binding to the viral DNA, polypeptide V can also bind to penton base and to the minor coat protein VI, linking the core to the capsid (15–16,23). Estimates on the copy number of protein μ (9 kDa, 21% Arg) (19) range between 100 and 300 copies per viral particle. Both polypeptide VII and μ are cleaved by the viral protease during maturation (24). Cross-linking studies have revealed interactions between polypeptides V and VII, V and μ, and all three proteins in viral cores (25).

There are no structural data for any of the adenovirus core proteins. It is not known how the 12 μm long molecule of dsDNA, bound to 20–25 MDa of protein, fits into the ∼0.1 μm diameter capsid. Two models have been proposed for the organization of the adenovirus core, based on assays carried out under different degrees of capsid disruption. Cross-linking, early electron microscopy (EM) and ion etching studies suggested that the dsDNA and proteins were organized as a cluster of 12 uniformly sized spheres (23 nm diameter), named 'adenosomes', located beneath the capsid vertices (26–28). An alternative chromatin-like model was proposed based on nuclease digestion experiments and Pt/C shadowing EM images of released cores showing a beaded appearance (29–31). According to these studies, the adenovirus core would be organized into ∼180–200 nucleosome-like subunits with an average diameter of 9.5 nm, for which also the name 'adenosome' was adopted. The main component of the adenosome would be polypeptide VII, with polypeptide V occupying the inter-adenosome DNA spacings. These spacings were highly variable in length, from 10 to 130 nm, although the most frequent distance between adenosomes was in the 10–15 nm range (31). Under milder disruption conditions, the adenosome beaded string formed a thicker fiber (15–30 nm) containing also polypeptide μ. A thick fiber has also been observed in disrupted immature adenovirus particles, containing the precursor version of μ (32). In the context of the different architectural roles of DNA-condensing proteins, these observations suggest that polypeptide VII could be acting as a wrapper, while μ might be a bridger. Finally, small-angle neutron and X-ray scattering experiments showed evidence of some ordering in the HAdV-C2 core, with a maximum in the scattering pattern at $1/29$ Å^{-1} (33).

Long range organization of the adenovirus core admits a certain degree of flexibility with regards to protein contents, as fusion of core proteins V or VII with green fluorescent protein (GFP) were tolerated for completion of the viral cycle (34,35). Deletion of polypeptide V resulted in low thermostability, but interestingly, this defect could be rescued through point mutations in polypeptide μ (36). The situation is the opposite with respect to DNA: viral variants with genomes below 75% or above 105% the length of the wild-type genome are genetically unstable and tend to undergo rearrangements to revert to 100% genome length (37). Further, genome deletions of ∼5 kbp (15% the total genome length) decrease particle thermostability (38).

Icosahedrally averaged cryo-EM maps (reviewed in (39)) have not revealed any hint of large, ordered spheres inside the adenovirus capsid. Instead, essentially homogeneous density is observed in the core, lacking the notable variations found in cryo-EM maps of other dsDNA viruses such as bacteriophage, herpesviruses or the adenovirus structurally related tectiviruses (40–42). These feature internal onion-like, shelled DNA density in the vicinity of the capsid, produced in some cases by the spooling of the genome around central proteic axes. However, none of these viruses package their genome in the presence of histone-like proteins like adenovirus. Here we extract the adenosome positions from cryo-electron tomography (cryo-ET) maps of intact, single, non-icosahedrally averaged adenovirus particles, and combine the data with statistical analysis and molecular dynamics (MD) simulations of two different effective models of adenosomes, which enable us to extract some of the physical properties underlying the organization of the core.

MATERIALS AND METHODS

Preparation of adenoviruses

The E1-deleted HAdV-C5 variant Ad5GL (43) was propagated in HEK293 cells. Ad5GL expresses GFP and firefly luciferase from the E1 region, and is completely wild type for all structural polypeptides. Particles were purified by equilibrium centrifugation in CsCl gradients, desalted on a Bio-Rad 10 DC column and stored in 20 mm Hepes, pH 7.8, 150 mm NaCl plus 10% glycerol at −70°C. Virus titer was 5×10^{12} virus particles (vp)/ml, as estimated by absorbance at 260 nm (44).

Cryo-electron tomography and image analysis

Viral samples were mixed at a concentration of 1×10^{12} vp/ml with 10-nm colloidal gold particles (AURION, Wageningen, The Netherlands) and vitrified as described (45). A Tecnai-12 electron microscope (FEI, Hillsboro, OR, USA) operating at 120 kV with a LaB_6 source and equipped with an energy filter (GIF 2002; Gatan, Pleasanton, CA, USA) was used to collect tilt series at ∼4 μm underfocus, covering the range ±70° in 2° increments. The data were acquired using the SerialEM package (46), for a total dose of ∼70–80 electrons/Å^2 per series. Images were recorded on a 2048×2048-pixel CCD camera (Gatan, Pleasanton, CA, USA) at ×38 500 magnification (7.8 Å/pixel). Data were preprocessed and aligned using the IMOD software package (47), with gold particles as fiducial markers.

The final aligned tilt series were normalized and reconstructed using the simultaneous iterative reconstruction technique implemented in Tomo3D (48). Individual virus particles were extracted from tomograms using IMOD. Tomograms were denoised by 100 iterations of anisotropic nonlinear diffusion (49). The in-plane resolution of the full tomograms was in the 43–55 Å range, as estimated using the Bsoft program TOMRES (50). The extracted viruses were aligned to an icosahedral reference using maximum likelihood procedures for tomography as implemented in XMIPP (51,52).

Adenosome positions in each virus particle were defined by manual picking in the original, extracted 3D map (subtomogram) using IMOD. Only regions with gray levels higher than those of the background (outside the virus particle) were considered to represent adenosomes. Afterward, those positions were transformed according to the subtomogram alignment parameters so as to represent the adenosome positions in the aligned viruses. Panel (c) in Figure 1 was created with UCSF Chimera (53).

Scaling of the radial distribution function

The distributions of interparticle distances were calculated from a dataset consisting of pairwise distances for *all pairs* of adenosomes within each viral particle, then averaged across the 20 viral particle maps. The maximal inter-adenosome distance d is ∼70 nm, the internal diameter of the capsid. The number of adenosome pairs at large distances becomes progressively smaller, which simply reflects the finite size of the viral core. To obtain a quantity characteristic only of the interactions between the adenosomes and without the influence of finite size effects, we need to appropriately scale the distributions. The resulting *scaled* radial distribution function (RDF) should saturate to one at large interparticle distances and can then be compared with its well-known counterparts in bulk materials (54). The scaling requires a calculation of the cluster shape factor, $f(d)$. For a spherical cluster of radius R_c (55) the cluster shape factor is given by

$$f(d) = \left(1 - \frac{d}{2R_c}\right)^2 \left(1 + \frac{d}{4R_c}\right); d < R_c. \quad (1)$$

Scaling of experimental data with the shape factor for a sphere produced the desired behavior of RDFs at large distances. When a numerically obtained scaling factor $f(d)$ for an icosahedron was used, there were no noticeable differences. We may thus treat the adenosome cluster shape as a sphere. As a 'bonus', the shape factor also enables us to determine the effective radius of the adenosome cluster ($R_c = 35 \pm 2$ nm (SE)), since the requirement that the RDF reduces to unity for large interparticle distances fixes the appropriate value of R_c. Small changes in R_c cause large deviations in RDF as d approaches $2R_c$, which enables us to pinpoint R_c with some precision. Note also that the experimental data exhibit pronounced noise as d approaches $2R_c$, as there are few pairs available there and the sampling is poor. For this reason the RDFs in Figure 3 are shown only up to 60 nm, as the RDFs in the interval of $60<d<72$ are dominated by noise augmented by $f(d)$.

Molecular dynamics

MD was performed in LAMMPS Molecular Dynamics Simulator (56) using a Langevin thermostat (57) with 230 interacting particles in confinement at room temperature k_BT. Sampling of the MD data was done after a sufficiently long equilibration/thermalization run—200 simulation samples were taken during 2×10^6 Verlet time-steps and statistically averaged over 50 different runs with random starting conditions. To identify effects related solely to the specific nature of the geometry, in all the simulations presented we have preserved the icosahedral symmetry of the confinement. The confining icosahedron interacts with the adenosome particles via a superposition of a soft repulsive Morse potential and a repulsive potential of the Weeks-Chandler-Andersen type (58). The range of the hard potential was chosen to be extremely small so as to properly mimic a hard wall, while the soft potential parameters were found by fitting the numerical data to the experimental, maintaining the hard wall fixed. Other specifics of the simulation are detailed in the corresponding sections.

Parameters of the inter-adenosome and adenosome-capsid potentials

The effective potential we used in the model of fluid of soft adenosomes is a shifted Morse potential,

$$v_r(d) = \begin{cases} D\left[e^{-2\kappa(d-d_0)} - 2e^{-\kappa(d-d_0)} + 1\right], & d < d_0; \\ 0, & d > d_0. \end{cases} \quad (2)$$

where d is the separation between adenosomes and d_0 is the potential cut-off radius. Comparison of the results of the MD simulations with the experimental data yielded the best-fit potential parameters $D \approx 1k_BT$, $d_0 \approx 11$ nm and $\kappa \approx 0.08$ nm^{-1}. The soft part of the capsid-adenosome interaction is well modeled with the same cut-off distance but with a smaller $\kappa \approx 0.055$ nm^{-1} (and a short-range hard-core repulsion enforcing the impenetrability of the confinement).

The adenosomes in the 'beads on a string' model are also connected along the chain with the harmonic potential given as

$$v_s(d) = \frac{k}{2}(d - l_0)^2, \quad (3)$$

where l_0 is the equilibrium length of the spring and k is the bond spring constant. The equilibrium 'bond' length chosen in this model (l_0) cannot be completely arbitrary, since there is a finite amount of DNA in the adenovirus. The two most important mechanisms for shortening of the bond length d-l_0 are the DNA molecule stretching and bending. The energy required to bend a straight DNA piece of length l_0 to an arc of radius R is

$$F_b = k_B T \frac{1}{2} \frac{l_p l_0}{R^2} \quad (4)$$

with $l_p \approx 50$ nm the persistence length of DNA. This can be expanded for small changes in the curvature $1/R$ to obtain:

$$\frac{F_b}{k_B T} = \frac{12 l_p}{l_0^2} (l_0 - l) = c\,(l_0 - l)\,, \quad (5)$$

where l is the linear distance between the DNA ending points in the bent state. As the potential energy dependence on the extension l_0-l is linear (it is a quadratic function of l_0/R) we match the two potentials $\frac{1}{2}k(\Delta l)^2 = c\,(l_0 - l)$ for different plausible extensions $\Delta l = 1$,2,5 nm. For $l_p =$ 50 nm and $l_0 = 19$ nm we find $k \sim 3$,1.6,0.7 $k_B T/\text{nm}^2$. In the case of stretching, the bond constant was found to be $k \sim 10$–$100 k_B T/\text{nm}^2$ after matching a molecular dynamics harmonic potential model to experimental data for DNA (59).

RESULTS

Statistical analysis of adenosome positions

In cryo-ET maps of single adenovirus particles, the core presented a punctate pattern, with variably sized regions displaying gray levels similar to those of the icosahedral shell, embedded in a weaker density background (Figure 1a). This pattern is consistent with previous data indicating a beaded pattern in the DNA–protein core complex when extracted from the capsid (30,31), and not with the model consisting of 12 large spheres. We hypothesized that each high density region corresponded to an adenosome (in the sense used in (31)), and manually determined the center of each one by visual inspection of the individual virus maps in 3D (Figure 1b and c). Weaker densities between adenosomes did not seem to follow a definite pattern. Statistical analysis of the adenosome positions was performed on 20 virion cores. The adenosome selection procedure yielded between 190 and 280 positions per viral particle corresponding to the center of regions of high density within the core, with a mean across all analyzed particles of $N = 230 \pm 30$ (SE), also consistent with previous observations on disrupted cores (30).

Visual inspection of the cryo-EM maps already indicated lack of pronounced order or symmetry in the core. To confirm this point, we first checked if there was any asymmetry in the distribution of adenosome positions. The adenosome coordinates were represented in a coordinate system with the z-axis directed along the line connecting two opposite capsid icosahedral vertices, and the origin of coordinates was set at the center of mass for each adenosome cluster (i.e. the set of adenosome positions for each viral particle). Projections of the data on the alignment axis and the perpendicular plane did not show any sign of preferred direction

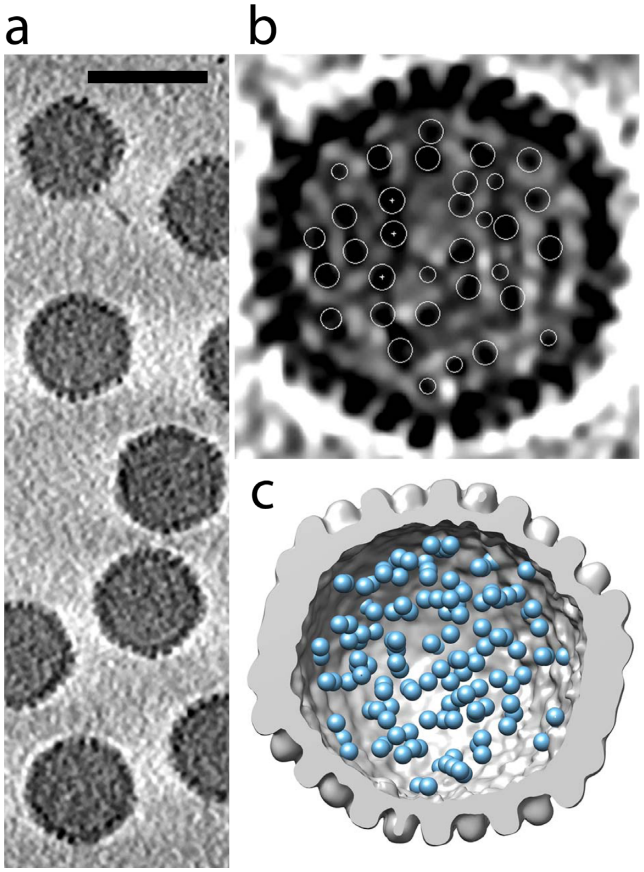

Figure 1. (**a**) Central section of a representative tomogram showing the punctate pattern in the adenovirus core. The bar represents 100 nm. (**b**) Central section of a single virus particle. The highest density regions are shown in black. Densities identified as adenosomes are encircled in white. Notice that circular outlines have different radii because they are cross-sections of spherical markers used for picking the adenosome centers in 3D. Central white dots in some of the circles correspond to the center of the spherical marker, i.e. the adenosome position as used for statistical analyses. (**c**) Surface rendering showing the adenovirus capsid cut open, obtained from averaging 20 individual virus tomograms after aligning with respect to an icosahedral reference (gray). The core density has been computationally removed and in its place, cyan spheres 4.5 nm in diameter indicate the positions of adenosomes for the viral particle shown in (b).

(Figure 2a). To assess whether there were some remnants of icosahedral symmetry, a fast Fourier transform (FFT) of the distribution of azimuthal angles was calculated for each virion and then averaged. No sign of 5-fold symmetry was found (Figure 2b). We conclude that the particles in each virus can be taken as forming a spherical cluster with respect to their center of mass.

In spite of the absence of pronounced order observed, additional statistical analyses indicated that the adenosome distribution differed from that of a randomly distributed set of points within an icosahedral enclosure (Figure 3a–c). First, we constructed RDF for the adenosomes in all viruses. The RDF represents the probability of finding two particles at a center-to-center distance d, calculated for *all* particle pairs in each adenosome cluster (each viral core). The distributions obtained from experimental data were averaged across 20 different adenovirus particles. The same

procedure was applied to the experimental data in all the indicators constructed. A further scaling of the data was performed in order to account for the finite size effects (see Materials and Methods). The procedure applied also gives an effective radius of the adenosome cluster, $R_c = 35 \pm 2$ nm (SE), a value consistent with that estimated for the core diameter from cryo-EM images (65 nm) (32).

RDFs indicate an effective repulsive nature of the adenosome–adenosome interaction at small distances, featuring a characteristic depletion for distances smaller than 8 nm where no pairs are observed (compare with the constant distribution corresponding to 230 randomly distributed dots in an icosahedron of mid-radius 35 nm—icosahedron reference calculation in Figure 3a). The slow decay of probability as d approaches zero indicates a very soft interaction potential (55). The RDF reduces from ∼1 to ∼0.5 in a radial interval of 3 nm (from $d \sim 8$ nm to $d \sim 5$ nm), and reaches 0.1 at $d = 3.5$ nm below which there is practically no probability of finding a particle pair. This leads us to define a hard particle diameter of ∼4 nm (effectively impenetrable) and a soft diameter of ∼10 nm, where the RDFs start to decay. In their study of X-ray scattering on HAdV-C2, Devaux *et al.* (33) reported a scattering maximum corresponding to 2.9 nm which could be interpreted as the hard core of our soft adenosomes. Alternatively, it is possible that this lower limit is a direct consequence of the imaging technique used, as this distance is in the same range as the in-plane resolution of our tomograms (see Materials and Methods). One should also note a small-amplitude, yet persistent peak at 10 nm, suggesting a very weak degree of adenosome first neighbor positional correlation—something expected for a fluid-like state. Beads of 9.5 nm diameter connected by variable lengths of dsDNA had been observed in disrupted cores (31). This is comparable with the soft diameter estimate obtained here. It should be mentioned here that, by 'soft' and 'hard' diameter, we do not mean that the adenosome proteins can be extensively compressed. Rather, we refer to the fact that a central protein core in the adenosome may be surrounded by DNA density susceptible to rearrangements.

As a second indicator of the core organization, we analyzed the distribution $p(d_{NN})$ of nearest neighbor distances d_{NN} for all the adenosomes in a virus, normalized so that its integral over d_{NN} is one. As Figure 3b shows, when compared against the random icosahedron reference calculation (effectively an *ideal gas* of adenosome particles), one observes that the mean value of the adenosome distribution, $\bar{d}_{NN}$, is displaced (outward) by ∼2 nm from that expected for a random distribution, which is essentially fixed by the point density, $\bar{d}_{NN}^{\text{rand}} \sim \sqrt[3]{2/(3N)}\,R_c$. This is a consequence of the repulsive nature of the inter-adenosome interaction revealed by the RDF, which pushes them further apart than for a random distribution, leading also to a narrower probability distribution of the nearest neighbor distances.

Finally, as a third indicator, we analyzed the density $\rho(r)$ of adenosome positions as a function of the distance from the cluster center of mass, r (Figure 3c). The density was calculated as the number of experimental positions per volume unit in each spherical shell. Density model curves are calculated in such a way that the curve integral will give the total number of positions in the dataset (the same for all presented curves). The adenosome density is nearly constant between radii 5 and 30 nm. A decrease of density is observed in regions with large radial distances—this is partially a geometric effect, due to reduction of available volume in the icosahedron as the radius increases from that of the inscribed sphere to that corresponding to the circumscribed sphere.

Modeling the adenosome interactions

Additional information on the adenovirus core can be extracted from the physical model of adenosome interaction constructed to reproduce the experimental data. The system we are dealing with consists of condensing proteins interacting with the DNA, confined in the capsid and immersed in a salt solution. In view of the lack of information on the conformation of the condensing proteins, we opted for simple models that reproduce basic features of the experimental data.

Adenosomes as a fluid with short-ranged soft repulsive interactions

The simplest model tested represents the adenosomes as a fluid with soft repulsive interactions, confined in a capsid with which it also interacts repulsively. This means that the details of the DNA packing are completely smeared, i.e. the DNA only renormalizes the inter-adenosome interactions. This does not mean that a possible pronounced association of the condensing proteins and the DNA is not accounted for by the model. The model can indeed account for such effects, but only in the short-range sense. The protein–DNA association can be included in the effective potential, but no topological constraints related to the finite length of DNA or to its elasticity survive in the coarse-grained representation.

In the soft repulsive fluid model, interactions between adenosomes are represented by a potential function $v_r(d)$, where d is the separation between adenosomes. As a sufficiently simple model for $v_r(d)$, we chose the shifted Morse potential (see Materials and Methods) and determined the parameters of the potential that best fit the experimental data using MD simulations. We have also considered other models for $v_r(d)$, and we find that the pronounced *softness* of the potential is its robust feature, regardless of the model used. The model of very soft, disconnected quasi-particles reproduces very satisfactorily the RDF (Figure 3d) and the nearest neighbor distance distribution (Figure 3e) observed in experiments. The only (slight) deviation from the experimental data is seen in the density $\rho(r)$ near the capsid wall at 30–40 nm (Figure 3f)—there we see a slower decay of the experimental density than predicted by the simulation. This may indicate that the effective confining potential induced by the capsid has a complicated spatial dependence, rendering the regions just below the icosahedron vertices more approachable to the adenosomes than those below the icosahedron sides. Additionally, we have assumed that the effective inter-adenosome potentials are independent of their position in the capsid. As these potentials are mediated by the DNA background, it seems likely that they will be different when the two adenosomes are close to the capsid than when

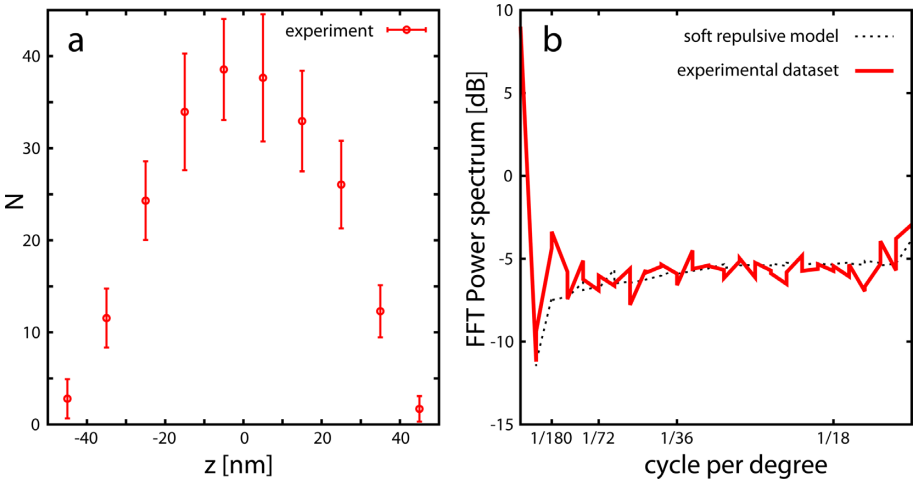

Figure 2. (**a**) Histogram of the averaged probability for finding adenosome particles in a horizontal slice, i.e. when all the particle positions are projected on the z-axis. For each viral particle, the origin of the coordinate system was set at the center of mass of the adenosome cluster. (**b**) FFT of the binned distribution of adenosome particle azimuthal coordinates for the soft repulsive fluid model (dotted line) and experimental dataset (full line). No difference is seen between the predictions of the repulsive fluid model and the experimental dataset.

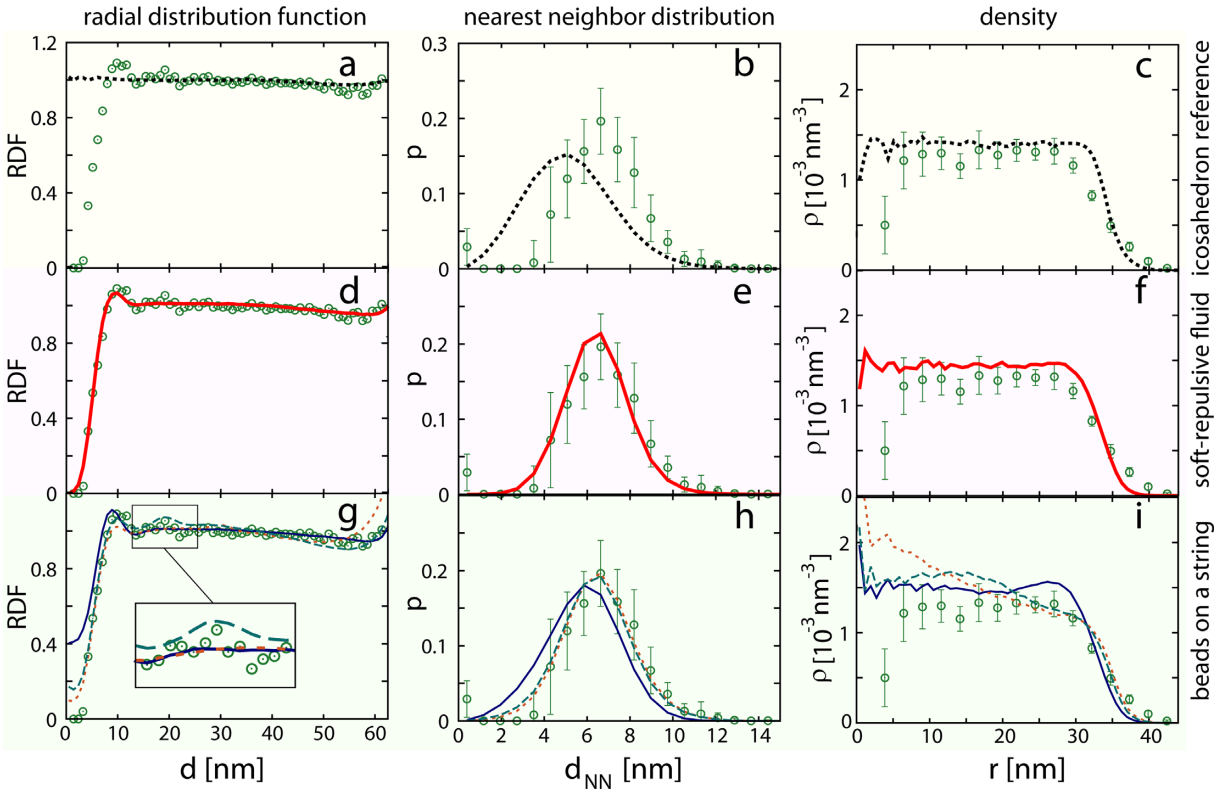

Figure 3. Statistical indicators of the adenosome position dataset, and their comparison with expected values for different theoretical models. The three statistical indicators (RDF, nearest neighbor distance distribution and density distribution, one per column) constructed from experimental data on adenosome positions are represented by green circles. The simulations performed with three different models are shown by rows. Top row: random icosahedron reference (dotted line). Middle row: soft repulsive fluid (full line). Bottom row: model of beads on a string. The full, dashed and dotted lines in (**g**) to (**i**) show the results for equilibrium bond lengths $l_0 = 8$ nm, 19 nm and 30 nm, respectively.

they are deep in the bulk of the core. Repulsive interactions result in an outward pressure on the capsid, estimated from the simulations as 0.055 ± 0.002 atm. We consider this value a lower bound, as it almost certainly does not include all the relevant contributions to the true pressure (see the Supporting material).

Adenosomes as a regular array of beads on a string

If the adenosomes are similar to nucleosomes (60), then the appropriate model would consist of quasi-particles linked together by the DNA to form an effective polymer. We may model the DNA 'background' in this case as a yardstick, imposing certain distances between the proteins along the chain (equilibrium bond length, l_0, constant throughout the chain). In such a model, any increase or decrease of the interprotein distance would require energy, the parabolic dependence on the change of distance being the simplest choice. So, in addition to the soft adenosome repulsion, $v_r(d)$, that acts between all of the adenosome pairs, in this model the adenosomes are also connected along the chain with a harmonic potential between two neighboring adenosomes (see Materials and Methods). The harmonic potential is characterized by the spring constant k and equilibrium bond length l_0. The equilibrium bond length chosen in this model cannot be completely arbitrary, since there is a finite amount of DNA in the adenovirus core. The upper limit is thus $l_0^{\max} = 12\ \mu\text{m}/230 = 52$ nm, but this does not include any DNA associated with (wrapped around) the condensing proteins. With effective diameter of the condensing proteins ~4.5 nm, a single wrap of DNA on the protein uses up $\sim 2(4.5/2+2.5/2)\pi \approx 22$ nm, so that the length of DNA remaining for linking the two adenosomes is 52–22 = 30 nm.

Bond lengths chosen for representative calculations were 30 nm, 8 nm and 19 nm, corresponding to approximately one turn of DNA around the adenosome; the shortest possible DNA linkage length consistent with the experimental data; and a value in between. The value of 8 nm is consistent with the proposed minimal contact distance between two adenosomes, e.g. as seen in the dimensions of beaded strings in disrupted cores (31); while still shorter bonds significantly modify the exclusion zone in the RDFs. Stiff bonds (large k) show up as clear maxima at $\sim l_0$ in RDFs due to distance correlations imposed by the bond length. This result that we find in our simulations (with large k's) is contrary to what is seen in experiments (no pronounced maxima in RDF), and we conclude that the inter-adenosome bonds, if they exist, must be very easy to stretch and compress (weak) in thermal equilibrium. In that case, the correlations between the adenosome positions are thermally smeared and the linkage, although present may not be seen in the indicators.

Assuming a straight linker piece of DNA, the energetics of its lengthening (DNA stretching) and shortening (DNA bending; note that the persistence length of DNA should be ~50 nm in experimental conditions) can be estimated and approximately related to the bond constant of a simple harmonic bond. This gives $k \sim 10\, k_B T/\text{nm}^2$ and $k \sim 1\, k_B T/\text{nm}^2$ for stretching and bending respectively (see Materials and Methods), both of which are quite stiff and produce significant correlations in the RDFs. However, different and more complicated *effective* bonds can be envisaged in a crowded (see the Supporting material) and strongly confined environment, and soft harmonic springs may mimic such a situation. That is why we have chosen a bond constant $k \approx 0.05\ k_B T/\text{nm}^2$, a smallest value that still yields noticeable disagreement with at least one experimental indicator. This value of the elastic constant is almost *two orders of magnitude* smaller than the conservative estimate for DNA bending.

Results presented in Figure 3g, h and i indicate that the existence of any type of bond worsens the agreement with the experimental data. Soft 8 nm bonds shift the nearest neighbor distance away from the experimental data because a short bond forces spatial nearest neighbors to also be the nearest neighbors on the bead-string backbone. One also observes a stronger correlation peak in the RDF with a corresponding 'anti-correlation' peak at ≈15 nm—although such a bond could be hidden in the experimental RDF it produces clear changes in the nearest neighbor distribution. The density (Figure 3i) shows a peak near the capsid surface due to an increased order imposed by confining a 'polymer' (61). If we take a larger bond equilibrium length of $l_0 = 30$ nm, we see that the RDF deviates from unity at large interparticle distances—adenosomes do not conform to a spherical cluster. This is easily explained, as a bond length comparable to the capsid diameter requires that the adenosomes explore the space beneath the icosahedron vertices to minimize their free energy. Also, there is a reduction of density around 10 nm from the capsid wall, inconsistent with the experimental data (Figure 3i). The model with 19 nm bond lengths shows a combination of these characteristic effects with the addition of a correlation peak in the RDF at the bond length (Figure 3g, inset). Irrespective of the equilibrium bond lengths chosen, the model of beads on a string is in worse compliance with the experimental data than the model of a fluid of soft interacting particles.

DISCUSSION

Packing of viral genomes inside protein shells presents the intriguing problem of compacting a long and highly charged polymer into a small space. Most of the available information on how viral genomes are packed comes from cases where genome-capsid contacts force their icosahedral ordering, at least in the outermost shells (9). The most striking cases come from the world of ssRNA viruses; for example, in the crystal structure of the small (170 Å) ssRNA Satellite Tobacco Mosaic virus, up to 45% of the genome was solved, closely interacting with the interior face of the T = 1 capsid. In a T = 3 Nodavirus, ordered RNA was seen to form a dodecahedral cage underneath the capsid shell, accounting for ~30% of the genome. Concentric shells of density, indicating a certain degree of order in the dsRNA genome packing, have also been seen in crystal structures of the larger Reoviridae. In the case of dsDNA viruses, cryo-EM studies have shown concentric density shells with a periodicity of ~25 Å in bacteriophage and herpesvirus (40–42), consistent with tightly packed duplex DNA. In the Podoviridae, the DNA molecule forms a coaxial spool by coiling around a large cluster of proteins inside the packaging vertex (62).

Bacteriophage and herpesvirus package naked dsDNA, while other viruses package dsDNA in complex with a considerable amount of protein. Such is the case of polyomaviruses, whose 5 kbp genome is condensed in ∼20 nucleosome structures by cellular histones, thus forming a minichromosome (10). There is no evidence of order in the viral core, even in the areas closely apposed to the inner capsid surface (63). The only information regarding the geometry of packing of this minichromosome within the virion comes from a combination of SAXS and coarse-grained modeling (64). These suggested a slightly higher chromatin density at the center of the viral particle, with the model that best fitted the data assuming loosely tethered nucleosomes. Adenovirus, analyzed here, has an eight times larger internal volume (35 versus 18 nm radius) and seven times larger genome, and presents a more complicated situation, with a large variety of DNA binding proteins packed together with the DNA, whose structural details (unlike those of the nucleosome histones) are unknown.

Here we show the first glimpse of the adenovirus adenosomes directly imaged in their physiological environment, the viral core. This is the first study addressing the interactions present in a viral protein–DNA condensate within the confining capsid. We found no strict type of ordering in the adenosome positions inside the capsid. Adenosomes exist as a fluid of soft particles without a strictly (and stiffly) defined DNA backbone. The DNA appears to act only as an effective medium for the soft inter-adenosome interactions in the crowded environment. The essential feature of adenosomes is a soft repulsive interaction they impose on neighboring adenosomes, so that they, to a first approximation, behave as a fluid of soft repulsive spheres. This interaction results in a finite excluded volume, and the nearest neighbor distance distribution shifted to larger values than would be expected for random points in an icosahedron. The range of the repulsive interaction (given approximately by $1/2\kappa$ in Equation (2)) is quite large, ∼6 nm, significantly larger than the range of electrostatic interaction in the Debye-Huckel approximation (∼1 nm at 150 mM salt concentration). The simplest model of adenovirus core that accounts for most of the indicators analyzed is that of hard spheres (condensing proteins) immersed in a 'soup' of DNA where the DNA mediates an effective soft repulsive interaction. There may be only a minor difference between this model and the experimental data, as seen in the density of adenosomes near the capsid surface.

The soft repulsion between adenosomes gives a modest internal pressure in the adenovirus capsid. Internal pressure has been measured or estimated inside other dsDNA viruses (bacteriophage and herpesvirus) and it appears to originate from the strong repulsion between the nucleic acid duplexes in close proximity (42,65). For adenovirus, the model described here predicts a lower bound of 0.055 ± 0.002 (SE) atm for the outward pressure. It is not clear at present if such a modest outward pressure would play a role in the initial stages of adenovirus uncoating (66), but it should be mentioned that there are additional contributions to the pressure, not accounted for by the model. These can be approximately estimated to obtain a total pressure of about ∼0.12 atm based on screened DNA charge interactions (see the Supporting material) (67). This is still at least an order of magnitude smaller than in the case of unscreened DNA charge interactions, observed in some bacteriophage (42). This estimate correlates with the fact that the dsDNA charges in adenovirus are probably shielded by the histone-like core proteins.

No evidence of a strict yardstick-like linkage between the adenosomes is seen in any of the experimental indicators—the data can be adequately explained by using the previous model of soft particles in confinement. The numerical (61) studies, however, do not strictly exclude other types of 'links': (i) extremely weak bonds (as those we investigated), (ii) a *distribution* of bond lengths where adenosomes slide along the contour, (iii) sliding bonds where the total length of non-bound DNA fluctuates—in dynamical terms, this signifies easier rearrangement of adenosomes in the DNA background than would be expected if they were tied together by stiff linker DNA pieces. The existence of adenosome filaments after disrupting the virion (30,31) does imply some kind of 'springs' between the adenosomes. Such interactions in disrupted cores, however, do not necessarily imply the same inside the crowded environment of the core within the intact capsid (68). Crowding shifts the equilibrium constant in DNA–protein interactions and may also induce non-canonical DNA structures (69,70). While the DNA indubitably makes a contribution to the core organization, in the intact particle this contribution is not reflected in stiff links between the proteins. Additionally, the possible bridging function of polypeptide μ (absent from the beaded structures in disrupted cores but present in the virion) may also be responsible for the differences observed.

DNA condensation by proteins is not a phenomenon exclusive to viruses: a similar process has to take place in cells, where very large genomes are condensed to various degrees into bacterial nucleoids or eukaryotic chromatin throughout cell cycles. In spite of many years of study, the interactions between nucleosomes that govern the organization of eukaryotic chromatin are still unclear. Similar to eukaryotes, some dsDNA viruses use histones or histone-like proteins to tightly condense their genome within the capsid shell. Adenovirus is not the only dsDNA virus encoding its own histone-like proteins. Recently, two large viruses infecting amoeba, Marseillevirus and Lausannevirus, have also been shown to encode histone-like proteins (71). Marseilllivirus and Laussanevirus are nucleocytoplasmic large DNA viruses (NCLDV), structurally related to adenovirus (72). Interestingly, organisms in the eukarya phylum Dinoflagellata diverge from the canonical chromatin organization in that they lack histones, but possess a positively charged, DNA binding protein co-localizing with chromosomes whose only known sequence similarity outside the phylum is to a Phycodnavirus protein (73). Phycodnaviridae also belong to the NCLDV class (72). Thus, studies on DNA condensation by viral histone-like proteins may help to understand the wide range of different mechanisms used for DNA compaction throughout Nature.

SUPPLEMENTARY DATA

Supplementary Data are available at NAR Online.

ACKNOWLEDGEMENTS

We are grateful to María López (CNB-CSIC) for expert technical help; Dr Juan Fontana (NIAMS, National Institutes of Health) for help with cryo-ET and Dr Alejandro Echeverría Rey for assistance with image processing.

FUNDING

Grants from the Ministerio de Economía y Competitividad of Spain [BFU2010-16382, BFU2013-41249-P (to C.S.M.), TIN2012-37483-C03-02 (to J.J.F.), BFU2011-29038 (to J.L.C.), and Spanish Interdisciplinary Network on the Biophysics of Viruses (Biofivinet, FIS2011-16090-E)]; Intramural Research Program of NIAMS (to A.C.S.). A.J.P.-B. was a recipient of a Juan de la Cierva postdoctoral contract from the Ministerio de Ciencia e Innovación of Spain and was additionally supported by a CSIC Travel Grant PA1002892. Funding for open access charge: BFU2013-41249-P from the Ministerio de Economía y Competitividad of Spain.
Conflict of interest statement. None declared.

REFERENCES

1. Marenduzzo,D., Finan,K. and Cook,P.R. (2006) The depletion attraction: an underappreciated force driving cellular organization. *J. Cell Biol.*, **175**, 681–686.
2. Richter,K., Nessling,M. and Lichter,P. (2007) Experimental evidence for the influence of molecular crowding on nuclear architecture. *J. Cell Sci.*, **120**, 1673–1680.
3. Hancock,R. (2012) Structure of metaphase chromosomes: a role for effects of macromolecular crowding. *PLoS One*, **7**, e36045.
4. Luijsterburg,M.S., White,M.F., van Driel,R. and Dame,R.T. (2008) The major architects of chromatin: architectural proteins in bacteria, archaea and eukaryotes. *Crit. Rev. Biochem. Mol. Biol.*, **43**, 393–418.
5. Carrivain,P., Cournac,A., Lavelle,C., Lesne,A., Mozziconacci,J., Paillusson,F., Signon,L., Victor,J.-M. and Barbi,M. (2012) Electrostatics of DNA compaction in viruses, bacteria and eukaryotes: functional insights and evolutionary perspective. *Soft Matter*, **8**, 9285–9301.
6. Uhlmann,F. (2014) A silent revolution in chromosome biology. *Nat. Rev. Mol. Cell Biol.*, **15**, 431.
7. Maeshima,K., Hihara,S. and Eltsov,M. (2010) Chromatin structure: does the 30-nm fibre exist in vivo? *Curr. Opin. Cell Biol.*, **22**, 291–297.
8. Garcia,H.G., Grayson,P., Han,L., Inamdar,M., Kondev,J., Nelson,P.C., Phillips,R., Widom,J. and Wiggins,P.A. (2007) Biological consequences of tightly bent DNA: the other life of a macromolecular celebrity. *Biopolymers*, **85**, 115–130.
9. Prasad,B.V.V. and Prevelige,P.E. Jr (2003) Viral genome organization. In: Richards,FM, Eisenberg,DS and Kuriyan,J (eds). *Virus Structure. Advances in Protein Chemistry*. Academic Press, San Diego, CA, Vol. **64**, pp. 219–258.
10. Germond,J.E., Hirt,B., Oudet,P., Gross-Bellark,M. and Chambon,P. (1975) Folding of the DNA double helix in chromatin-like structures from simian virus 40. *Proc. Natl Acad. Sci. U.S.A.*, **72**, 1843–1847.
11. Wold,W.S.M. and Horwitz,M.S. (2007) Adenoviruses. In: Knipe,D, Howley,PM, Griffin,DE, Lamb,RA and Martin,MA (eds). *Fields Virology*. 5th edn. Lippincott Williams & Wilkins, Philadelphia, PA, pp. 2395–2436.
12. Thomas,C.E., Ehrhardt,A. and Kay,M.A. (2003) Progress and problems with the use of viral vectors for gene therapy. *Nat. Rev. Genet.*, **4**, 346–358.
13. Liu,H., Jin,L., Koh,S.B., Atanasov,I., Schein,S., Wu,L. and Zhou,Z.H. (2010) Atomic structure of human adenovirus by cryo-EM reveals interactions among protein networks. *Science*, **329**, 1038–1043.
14. Giberson,A.N., Davidson,A.R. and Parks,R.J. (2012) Chromatin structure of adenovirus DNA throughout infection. *Nucleic Acids Res.*, **40**, 2369–2376.
15. Chatterjee,P.K., Vayda,M.E. and Flint,S.J. (1986) Identification of proteins and protein domains that contact DNA within adenovirus nucleoprotein cores by ultraviolet light crosslinking of oligonucleotides ^{32}P-labelled *in vivo*. *J. Mol. Biol.*, **188**, 23–37.
16. Pérez-Vargas,J., Vaughan,R.C., Houser,C., Hastie,K.M., Kao,C.C. and Nemerow,G.R. (2014) Isolation and characterization of the DNA and protein binding activities of adenovirus core protein V. *J. Virol.*, **88**, 9287–9296.
17. Chatterjee,P.K., Yang,U.C. and Flint,S.J. (1986) Comparison of the interactions of the adenovirus type 2 major core protein and its precursor with DNA. *Nucleic Acids Res.*, **14**, 2721–2735.
18. Johnson,J.S., Osheim,Y.N., Xue,Y., Emanuel,M.R., Lewis,P.W., Bankovich,A., Beyer,A.L. and Engel,D.A. (2004) Adenovirus protein VII condenses DNA, represses transcription, and associates with transcriptional activator E1A. *J. Virol.*, **78**, 6459–6468.
19. Anderson,C.W., Young,M.E. and Flint,S.J. (1989) Characterization of the adenovirus 2 virion protein, mu. *Virology*, **172**, 506–512.
20. van Oostrum,J. and Burnett,R.M. (1985) Molecular Composition of the Adenovirus Type-2 Virion. *J. Virol.*, **56**, 439–448.
21. Benevento,M., Di Palma,S., Snijder,J., Moyer,C.L., Reddy,V.S., Nemerow,G.R. and Heck,A.J. (2014) Adenovirus composition, proteolysis, and disassembly studied by in-depth qualitative and quantitative proteomics. *J. Biol. Chem.*, **289**, 11421–11430.
22. Burg,J.L., Schweitzer,J. and Daniell,E. (1983) Introduction of superhelical turns into DNA by adenoviral core proteins and chromatin assembly factors. *J. Virol.*, **46**, 749–755.
23. Everitt,E., Lutter,L. and Philipson,L. (1975) Structural proteins of adenoviruses. XII. Location and neighbor relationship among proteins of adenovirion type 2 as revealed by enzymatic iodination, immunoprecipitation and chemical cross-linking. *Virology*, **67**, 197–208.
24. Blainey,P.C., Graziano,V., Pérez-Berná,A.J., McGrath,W.J., Flint,S.J., Martín,C., Xie,X.S. and Mangel,W.F. (2013) Regulation of a Viral Proteinase by a Peptide and DNA in One-dimensional Space: IV. Viral proteinase slides along DNA to locate and process its substrates. *J. Biol. Chem.*, **288**, 2092–2102.
25. Chatterjee,P.K., Vayda,M.E. and Flint,S.J. (1985) Interactions among the three adenovirus core proteins. *J. Virol.*, **55**, 379–386.
26. Brown,D.T., Westphal,M., Burlingham,B.T., Winterhoff,U. and Doerfler,W. (1975) Structure and composition of the adenovirus type 2 core. *J. Virol.*, **16**, 366–387.
27. Newcomb,W.W., Boring,J.W. and Brown,J.C. (1984) Ion etching of human adenovirus 2: structure of the core. *J. Virol.*, **51**, 52–56.
28. Wong,M.L. and Hsu,M.T. (1989) Linear adenovirus DNA is organized into supercoiled domains in virus particles. *Nucleic Acids Res.*, **17**, 3535–3550.
29. Corden,J., Engelking,H.M. and Pearson,G.D. (1976) Chromatin-like organization of the adenovirus chromosome. *Proc. Natl Acad. Sci. U.S.A.*, **73**, 401–404.
30. Mirza,M.A. and Weber,J. (1982) Structure of adenovirus chromatin. *Biochim. Biophys. Acta*, **696**, 76–86.
31. Vayda,M.E., Rogers,A.E. and Flint,S.J. (1983) The structure of nucleoprotein cores released from adenovirions. *Nucleic Acids Res.*, **11**, 441–460.
32. Pérez-Berná,A.J., Marabini,R., Scheres,S.H.W., Menéndez-Conejero,R., Dmitriev,I.P., Curiel,D.T., Mangel,W.F., Flint,S.J. and San Martín,C. (2009) Structure and uncoating of immature adenovirus. *J. Mol. Biol.*, **392**, 547–557.
33. Devaux,C., Timmins,P.A. and Berthet-Colominas,C. (1983) Structural studies of adenovirus type 2 by neutron and X-ray scattering. *J. Mol. Biol.*, **167**, 119–132.
34. Le,L.P., Le,H.N., Nelson,A.R., Matthews,D.A., Yamamoto,M. and Curiel,D.T. (2006) Core labeling of adenovirus with EGFP. *Virology*, **351**, 291–302.
35. Puntener,D., Engelke,M.F., Ruzsics,Z., Strunze,S., Wilhelm,C. and Greber,U.F. (2011) Stepwise loss of fluorescent core protein V from human adenovirus during entry into cells. *J. Virol.*, **85**, 481–496.
36. Ugai,H., Borovjagin,A.V., Le,L.P., Wang,M. and Curiel,D.T. (2007) Thermostability/infectivity defect caused by deletion of the core protein V gene in human adenovirus type 5 is rescued by thermo-selectable mutations in the core protein X precursor. *J. Mol. Biol.*, **366**, 1142–1160.
37. Bett,A.J., Prevec,L. and Graham,F.L. (1993) Packaging capacity and stability of human adenovirus type 5 vectors. *J. Virol.*, **67**, 5911–5921.

38. Smith,A.C., Poulin,K.L. and Parks,R.J. (2009) DNA genome size affects the stability of the adenovirus virion. *J. Virol.*, **83**, 2025–2028.
39. San Martín,C. (2012) Latest Insights on Adenovirus Structure and Assembly. *Viruses*, **4**, 847–877.
40. Booy,F.P., Newcomb,W.W., Trus,B.L., Brown,J.C., Baker,T.S. and Steven,A.C. (1991) Liquid-crystalline, phage-like packing of encapsidated DNA in herpes simplex virus. *Cell*, **64**, 1007–1015.
41. San Martín,C., Burnett,R.M., de Haas,F., Heinkel,R., Rutten,T., Fuller,S.D., Butcher,S.J. and Bamford,D.H. (2001) Combined EM/X-ray imaging yields a quasi-atomic model of the adenovirus-related bacteriophage PRD1, and shows key capsid and membrane interactions. *Structure*, **9**, 917–930.
42. De Frutos,M., Leforestier,A. and Livolant,F. (2014) Relationship between the genome packaging in the bacteriophage capsid and the kinetics of DNA ejection. *Biophys. Rev. Lett.*, **9**, 81–104.
43. Seki,T., Dmitriev,I., Kashentseva,E., Takayama,K., Rots,M., Suzuki,K. and Curiel,D.T. (2002) Artificial extension of the adenovirus fiber shaft inhibits infectivity in coxsackievirus and adenovirus receptor-positive cell lines. *J. Virol.*, **76**, 1100–1108.
44. Maizel,J.V. Jr, White,D.O. and Scharff,M.D. (1968) The polypeptides of adenovirus. I. Evidence for multiple protein components in the virion and a comparison of types 2, 7A, and 12. *Virology*, **36**, 115–125.
45. Harris,A., Cardone,G., Winkler,D.C., Heymann,J.B., Brecher,M., White,J.M. and Steven,A.C. (2006) Influenza virus pleiomorphy characterized by cryoelectron tomography. *Proc. Natl Acad. Sci. U.S.A.*, **103**, 19123–19127.
46. Mastronarde,D.N. (2005) Automated electron microscope tomography using robust prediction of specimen movements. *J. Struct. Biol.*, **152**, 36–51.
47. Kremer,J.R., Mastronarde,D.N. and McIntosh,J.R. (1996) Computer visualization of three-dimensional image data using IMOD. *J. Struct. Biol.*, **116**, 71–76.
48. Agulleiro,J.I. and Fernandez,J.J. (2011) Fast tomographic reconstruction on multicore computers. *Bioinformatics*, **27**, 582–583.
49. Frangakis,A.S. and Hegerl,R. (2001) Noise reduction in electron tomographic reconstructions using nonlinear anisotropic diffusion. *J. Struct. Biol.*, **135**, 239–250.
50. Heymann,J.B., Cardone,G., Winkler,D.C. and Steven,A.C. (2008) Computational resources for cryo-electron tomography in Bsoft. *J. Struct. Biol.*, **161**, 232–242.
51. Scheres,S.H., Núñez-Ramírez,R., Sorzano,C.O., Carazo,J.M. and Marabini,R. (2008) Image processing for electron microscopy single-particle analysis using XMIPP. *Nat. Protoc.*, **3**, 977–990.
52. Scheres,S.H., Melero,R., Valle,M. and Carazo,J.-M. (2009) Averaging of electron subtomograms and random conical tilt reconstructions through likelihood optimization. *Structure*, **17**, 1563–1572.
53. Pettersen,E.F., Goddard,T.D., Huang,C.C., Couch,G.S., Greenblatt,D.M., Meng,E.C. and Ferrin,T.E. (2004) UCSF Chimera–a visualization system for exploratory research and analysis. *J. Comput. Chem.*, **25**, 1605–1612.
54. Likos,C.N. (2001) Effective interactions in soft condensed matter physics. *Phys. Rep.*, **348**, 267–439.
55. Lei,M., de Graff,A.M.R., Thorpe,M.F., Wells,S.A. and Sartbaeva,A. (2009) Uncovering the intrinsic geometry from the atomic pair distribution function of nanomaterials. *Phys. Rev. B*, **80**, 24118.
56. Plimpton,S. (1995) Fast parallel algorithms for short-range molecular dynamics. *J. Comput. Phys.*, **117**, 1–19.
57. Schneider,T. and Stoll,E. (1978) Molecular-dynamics study of a three-dimensional one-component model for distortive phase transitions. *Phys. Rev. B*, **17**, 1302–1322.
58. Weeks,J., Chandler,D. and Andersen,H. (1971) Role of Repulsive Forces in Determining the Equilibrium Structure of Simple Liquids. *J. Chem. Phys.*, **54**, 5237–5247.
59. Locker,C.R. and Harvey,S.C. (2006) A model for viral genome packing. *Multiscale Model. Simul.*, **5**, 1264–1279.
60. Schiessel,H. (2003) The physics of chromatin. *J. Phys.*, **15**, R699.
61. Jun,S., Arnold,A. and Ha,B.-Y. (2007) Confined space and effective interactions of multiple self-avoiding chains. *Phys. Rev. Lett.*, **98**, 128303.
62. Cuervo,A., Dauden,M.I. and Carrascosa,J.L. (2013) Nucleic acid packaging in viruses. *Subcell. Biochem.*, **68**, 361–394.
63. Baker,T.S., Drak,J. and Bina,M. (1988) Reconstruction of the three-dimensional structure of simian virus 40 and visualization of the chromatin core. *Proc. Natl Acad. Sci. U.S.A.*, **85**, 422–426.
64. Saper,G., Kler,S., Asor,R., Oppenheim,A., Raviv,U. and Harries,D. (2013) Effect of capsid confinement on the chromatin organization of the SV40 minichromosome. *Nucleic Acids Res.*, **41**, 1569–1580.
65. Bauer,D.W., Huffman,J.B., Homa,F.L. and Evilevitch,A. (2013) Herpes virus genome, the pressure is on. *J. Am. Chem. Soc.*, **135**, 11216–11221.
66. Pérez-Berná,A.J., Ortega-Esteban,A., Menéndez-Conejero,R., Winkler,D.C., Menéndez,M., Steven,A.C., Flint,S.J., de Pablo,P.J. and San Martín,C. (2012) The role of capsid maturation on adenovirus priming for sequential uncoating. *J. Biol. Chem.*, **287**, 31582–31595.
67. Šiber,A., Božič,A.L. and Podgornik,R. (2012) Energies and pressures in viruses: contribution of nonspecific electrostatic interactions. *Phys. Chem. Chem. Phys.*, **14**, 3746–3765.
68. Minton,A.P. (1997) Influence of excluded volume upon macromolecular structure and associations in 'crowded' media. *Curr. Opin. Biotechnol.*, **8**, 65–69.
69. Nakano,S., Miyoshi,D. and Sugimoto,N. (2014) Effects of molecular crowding on the structures, interactions, and functions of nucleic acids. *Chem. Rev.*, **114**, 2733–2758.
70. Zimmerman,S.B. (1993) Macromolecular crowding effects on macromolecular interactions: some implications for genome structure and function. *Biochim. Biophys. Acta*, **1216**, 175–185.
71. Thomas,V., Bertelli,C., Collyn,F., Casson,N., Telenti,A., Goesmann,A., Croxatto,A. and Greub,G. (2011) Lausannevirus, a giant amoebal virus encoding histone doublets. *Environ. Microbiol.*, **13**, 1454–1466.
72. Krupovic,M. and Bamford,D.H. (2008) Virus evolution: how far does the double beta-barrel viral lineage extend? *Nat. Rev. Microbiol.*, **6**, 941–948.
73. Gornik,S.G., Ford,K.L., Mulhern,T.D., Bacic,A., McFadden,G.I. and Waller,R.F. (2012) Loss of nucleosomal DNA condensation coincides with appearance of a novel nuclear protein in dinoflagellates. *Curr. Biol.*, **22**, 2303–2312.